NASA Contractor Report 3679

Effects of Specimen Resonances on Acoustic-Ultrasonic Testing

James H. Williams, Jr., Elsbeth B. Kahn,
and Samson S. Lee

GRANT NSG-3210
MARCH 1983

NASA

NASA Contractor Report 3679

Effects of Specimen Resonances on Acoustic-Ultrasonic Testing

James H. Williams, Jr., Elsbeth B. Kahn,
and Samson S. Lee
Massachusetts Institute of Technology
Cambridge, Massachusetts

Prepared for
Lewis Research Center
under Grant NSG-3210

National Aeronautics
and Space Administration

**Scientific and Technical
Information Branch**

1983

INTRODUCTION

Acoustic emission (AE) refers to the generation, propagation and detection of transient stress waves in materials as they undergo deformation or fracture. The stress waves propagate to the surface of the structure where they may be detected by an ultrasonic transducer. The output of the transducer is electronically processed and the resulting signal is interpreted as the "AE" signal. Acoustic emission has been found useful as a nondestructive evaluation (NDE) technique for the structural integrity assessment of metallic and nonmetallic structures [1-9].

In ultrasonic testing (UT) an ultrasonic stress wave is introduced into a structure and is measured after it has propagated through the structure [10]. Various NDE parameters based on UT have been found useful for the integrity assessment of structures. One such parameter is the through-thickness attenuation of the material which is a measure of the decrease in the amplitude of the stress wave as it propagates through the structure [8, 11-16]. Another UT parameter is called the "stress wave factor" [17,18] which involves the introduction of an ultrasonic spike into the structure and the reception of the resulting wave, with the transmitting and receiving transducers located on the same face of the structure [15].

The term acoustic-ultrasonic (AU) testing refers to NDE techniques that encompass both AE and UT. Many factors affect AU test results, such as specimen material and geometry, transducer characteristics, and measurement equipment. The objective of this work is to illustrate the enormous effects which specimen resonances can have on AU testing.

The frequency response of a solid aluminum block test specimen to the fracture of a mechanical pencil lead and the impact of two different diameter spheres are obtained from two different receiving transducer locations. Resonant frequencies and the corresponding normal mode nodal patterns of the block specimen are measured. The frequency spectra resulting from the fractures of the pencil lead and the impacts of the spheres are examined to determine the influence of the resonant frequencies and the corresponding mode shapes on these spectra.

Denny Miller, Frank Higgins and Min-Chung Jan let us use their facilities at the Engineering Research Center of Western Electric at Princeton, New Jersey.

SUMMARY OF LITERATURE ACKNOWLEDGING SPECIMEN RESONANCES

Frequency spectral analyses of signals obtained from AU testing provide an alternative to the commonly measured AU parameters [19-22]. From studies of spectral analyses, two major factors have emerged as significant influences on AU spectra: transducer frequency characteristics and test specimen resonances. Transducer resonance effects on AU signals have generally been well recognized and accepted. Specimen resonance effects, on the other hand, have frequently not been considered, and in many cases apparently not recognized.

A review of the AU literature that has acknowledged specimen resonances is given in [23]. The effects of specimen resonances have been considered by a few authors in the frequency spectral analyses of AE signals [24-30] and UT signals [28]. Theoretical estimations of specimen resonances have been based on simplified models of the structure [24,25,27,28,30]. No experimental confirmation of specimen resonances has been reported, however. In most cases, the frequency domain resolution has not been provided. Even in those cases where it has been given, the resolution is too crude, making it difficult to resolve distinct specimen resonances. Material and specimen descriptions, type of test, transducer type, transducer location, frequency domain representation, AU measurement system frequency range capability, frequency range reported, frequency domain resolution, theoretical calculation of specimen resonances, experimental confirmation of specimen resonances, and effects of transducer location for each reviewed paper have been summarized in a single table in [23].

TEST SPECIMEN, EQUIPMENT, AND EXPERIMENTAL PROCEDURES

TEST SPECIMEN

The test specimen was a square solid block of 6061-T6 aluminum (dimensions are shown in Fig. 1). The surface had a smooth ground finish (approximately equal to a 16G finish as measured with a Microfinish Comparitor). The block was set on a 2.54 cm (1 in) wide, 2.54 cm (1 in) thick, 25.4 x 25.4 cm (10 x 10 in) square rubber base for support and isolation. The block was supported on the rubber base for all experiments.

SPECIMEN RESPONSE TO FRACTURE OF PENCIL LEAD AND IMPACT OF SPHERES

Equipment

The equipment used for the input signal generation and the subsequent recording and processing of the transducer output signal included a receiving transducer (Panametrics Model V109 longitudinal type, sensitivity of -115 dB relative to 1 V/μBar in the vicinity of 0.1 MHz); a mechanical pencil lead fracture apparatus; 0.5 mm (0.02 in) diameter pencil lead (Pentel type HB); sphere release apparatus; spheres (stainless steel ball bearings, 0.159 cm (1/16 in) and 0.318 cm (1/8 in) diameter); filter (Rockland Systems Model 442 Dual Hi/Lo with a built-in amplifier); attenuator (Hewlett Packard Model 355C VHF and Hewlett Packard Model 355D VHF connected in series); epoxy (Devcon 5-minute 5-205) for mounting the receiving transducers; and a digital recording system. A schematic of the experimental system is shown in Fig. 2, where the sphere release apparatus is illustrated as the source of the input signal.

The digital recording system was designed and assembled at Western Electric's Engineering Research Center in Princeton, New Jersey. The system consisted of an 8-bit analog to digital converter interfaced to the direct memory access channel of a microcomputer (Cromemco). The maximum memory size available per signal was 64 K bytes (1 K byte = 1024 bytes). The system had a pre-trigger retaining 80 sample points prior to triggering to be included with the recorded signal. Off-line digital signal processing was conducted on a Digital Equipment VAX computer at MIT.

Procedure for Signal Conditioning

All signals were sampled at a rate of 1 MHz (one sample per

microsecond) using 64 K bytes of computer memory per signal, making each recorded signal 65.536 msec in duration. The trigger level was fixed for all measurements corresponding to 16 mV after total system amplification (amplification minus attenuation).

The signals were bandpass filtered from 10 to 280 kHz prior to analog to digital conversion. The highpass cutoff frequency of 10 kHz was chosen to eliminate any low frequency noise that might have resulted from machine or environmental sources. The lowpass cutoff of 280 kHz was chosen because it more than accommodated the predicted frequency components of the sphere impacts [23] based on the Hertz theory of impact [34,35], and it also satisfied the antialiasing requirement of allowing no frequency components greater than or equal to 500 kHz (the aliasing frequency [31-33]). For consistency and ease of comparison with frequency spectra due to sphere impacts, the pencil lead fracture signals were sampled with identical settings although the pencil lead fracture may contain a broader frequency spectrum [36,37]. The total system amplifications (amplification minus attenuation) for the pencil lead fracture, 0.159 cm (1/16 in) sphere impact, and 0.318 cm (1/8 in) sphere impact were 31, 34, and 21 dB, respectively, for both locations 1 and 2. (Refer to Fig. 1.)

Procedure for Pencil Lead Fracture

The transducer was mounted at output transducer location 1 (Fig. 1) with the epoxy. The mechanical pencil lead fracture apparatus which held the pencil on a rack and pinion assembly was positioned over the center of the block. The angle of inclination of the pencil, with respect to the vertical, was fixed at 40 degrees. This angle was chosen, by trial and error, to reduce sliding of the pencil lead across the block surface as the pencil was being lowered prior to fracture. This angle also allowed the fractured piece of lead to leave the block surface without bouncing, thus avoiding a second input signal. The pencil lead was extended approximately 2.5 mm (0.10 in). The pencil was positioned such that the tip of the extended lead aligned with the center of the input location (See Fig. 1). The pencil lead was fractured by lowering the pencil on th rack and pinion assembly using a rapid, smooth turn of the pinion gear. Care was taken to prevent the metal sleeve on the mechanical pencil tip from touching the block surface. The surface of the block was wiped clean with an acetone moistened cloth after each fracture. The pencil lead fracture was repeated a total of five times for output transducer location 1.

The pencil lead fracture tests were repeated for the receiving transducer mounted at output transducer location 2 (See Fig. 1).

Procedure for Sphere Impact

The sphere release apparatus which held the ball bearing with an electromagnet was positioned over the block. The 0.159 cm (1/16 in) diameter sphere was placed at a fixed location on the bottom side of the electromagnet. The center of the sphere was adjusted to height of 1.5 cm (0.59 in) from the surface of the block and aligned with the input location (See Fig. 1). The sphere was released from the electromagnet by depression of a switch. The sphere and block surface were cleaned with acetone after each impact. The first bounce of the 0.159 cm (1/16 in) sphere impact was recorded, for a total of five tests, at output transducer location 1.

The 0.318 cm (1/8 in) diameter sphere impacts were performed and recorded using the same procedures as for the 0.159 cm (1/16 in) sphere.

The procedures for the 0.159 cm (1/16 in) and 0.318 cm (1/8 in) sphere impacts were repeated for the receiving transducer mounted at output transducer location 2 (See Fig. 1).

MEASUREMENT OF NATURAL MODE SHAPES

Equipment

The equipment used for the measurement of nodal patterns and the outputvoltage amplitude of the receiving transducer included a signal generator (Tektronix Model FG 501); an oscilloscope (Tektronix Model 502A dual-beam); a digital frequency counter (Hewlett Packard Model 5381A 80 MHz); a source transducer (Panametrics Model V112 longitudinal type, sensitivity of less than -100 dB relative to 1 V/μBar in the vicinity of 0.1 MHz); a receiving transducer (Panametrics Model V109 longitudinal type); epoxy (Devcon 5-minute 5-205) for mounting the input transducers; and an output transducer-specimen interface couplant (Acoustic Emission Technology SC-6). A schematic of the experimental system is shown in Fig. 3.

Procedure for Measurement of Nodal Patterns

The nodal patterns were measured by the following procedure. A grid of 2.54 cm (1 in) squares was drawn on the top and one side of the block for spatial reference. The source transducer was epoxied in place at the input location (Fig. 1) on the top surface of the block. The top and one side of the block were coated with

a thin layer of couplant. The receiving transducer was placed on the top of the block close to, but not touching, the source transducer. The signal generator was set for a 15 V peak-to-peak sinusoidal output to the source transducer. The signal generator was tuned, while watching the oscilloscope, so that the maximum amplitude of the receiving transducer signal in proximity of the selected resonant frequency was obtained. The frequency at the maximum amplitude was recorded and maintained at this value throughout the measurement of the nodal pattern.

The output signal of the receiving transducer, displayed on the oscilloscope, was oriented so that a peak of the sinusoid was in the center of the screen. This orientation of the signal was arbitrarily assigned a positive phase. The receiving transducer was slowly moved across the top and side of the block while watching the oscilloscope. If a trough of the sinusoid shifted to the center of the screen a change of phase was noted on a sketch of the block with a corresponding grid pattern. The change of phase, positive to negative (peak to trough) or vice versa, indicated a nodal line had been crossed. After the receiving transducer had been made to transverse the top and side surfaces completely and all of the encountered phase shifts noted, the locations of the phase shifts were connected by smooth curves on the corresponding sketch. The resulting nodal pattern, consisting of the nodal lines, was confirmed experimentally by the presence of phase shifts at the expected locations. The nodal patterns for 16.42, 17.46, 21.11, 40.37, 50.95, and 75.64 kHz were obtained.

RESULTS AND DISCUSSION

TIME AND FREQUENCY DOMAIN REPRESENTATIONS

Time domain and frequency domain representations of the output signals are discussed in this section. All signal amplitudes, in the time domain and in the frequency domain, discussed are post-transducer amplitudes; that is, after the removal of the total system amplification from the recorded signals.

Time domain signals of the pencil lead fractures and sphere impacts were similar [23]. The signals had a general amplitude decay in time. The initial maximum peak-to-peak amplitude of the signals was of the order of 3 mV. After 30 msec, the maximum peak-to-peak amplitude of the signals was of the order of 0.05 mV.

The discrete Fourier transform (DFT) was calculated for the pencil lead fracture signal obtained at output transducer location 1 using 65536 points (65.536 msec) and again on the same signal using 32768 points (32.768 msec), or the first half of the recorded data points [38]. The magnitude spectrum calculated using 32768 points was slightly smoother in appearance than the spectrum calculated using 65536 points; other than this, the two spectra were identical. The difference in appearance was caused by the difference in resolution of the two spectra. The resolution is given by [31-33]

$$\text{Frequency Resolution (Hz)} = \frac{1}{NT} \tag{1}$$

where N is the total number of sample points and T is the sampling interval in seconds, which for the sampling rate of 1 MHz is 1 μsec here. The corresponding resolutions for the 65536 and 32768 point spectra are 15.25 Hz and 30.52 Hz, respectively. The fact that the two spectra, calculated with all of the data points and again with only the first half of the data points, were identical, indicated that the low amplitude signal present in the time-domain beyond 30.0 msec was not providing additional spectral information. Thus, all subsequent DFT calculations were made using the first 32768 (32.768 msec) of the measured data points.

Figs. 4(a) and 4(b) show the magnitude of the DFT from 10 to 80 kHz for the pencil lead fracture and the 0.159 cm (1/16 in) sphere impact, respectively, each obtained at location 1. The units of the magnitude spectrum are volts because [23,31-33]

$$F(\omega) = T\,\overline{F}_m \tag{2}$$

where $F(\omega)$ is the continuous Fourier transform, T is the sampling interval, and $\overline{F}_m$ is the discrete Fourier transform.

The spectra are broadband with greater magnitude at the lower frequencies [23]. For example, for the spectrum resulting from the pencil lead fracture, the DFT magnitude decreases to a maximum of approximately 0.05 V at 200 kHz. For the spectrum resulting from the 0.159 cm (1/16 in) diameter sphere impact, the DFT magnitude decreases to a maximum of approximately 0.005 V at 200 kHz. The shape of the spectrum resulting from the 0.318 cm (1/8 in) diameter sphere impact (not shown) is similar to that resulting from the 0.159 cm (1/16 in) diameter sphere impact, except for a general increase in the DFT magnitude.

Close examination of Fig. 4 reveals strong similarities between the two spectra. Peaks in both spectra appear at the respective corresponding frequencies. Similarly, peaks in spectra obtained at output transducer location 2 appear at the same frequencies for both pencil lead fractures and sphere impacts.

On the other hand, marked differences between the spectra obtained at locations 1 and 2 can be seen from Fig. 5 where the spectra from a pencil lead fracture recorded at locations 1 and 2 are shown in the frequency range of 10 to 30 kHz. High amplitude peaks at 17.46 and 21.11 kHz appearing in the spectrum from location 1 (Fig. 5(a)) appear at sharply reduced amplitudes in the spectrum from location 2 (Fig. 5(b)). A high amplitude peak at 16.42 kHz appears in the spectrum from location 2 but at a greatly reduced amplitude in the spectrum from location 1. These comments about the pencil lead fractures spectra apply equally to the sphere impacts spectra.

The pronounced similarities exhibited at either location 1 or at location 2 between the spectra resulting from the three different inputs suggests that the spectral content of the received signal is dominated by the natural frequency response of the test specimen itself and is influenced by the transducer location. Also, note that the marked differences between spectra at locations 1 and 2 from the same source lends further support to such a conclusion.

COMPARISON OF TEST SPECIMEN NATURAL FREQUENCIES WITH OUTPUT SPECTRA

Five predominant frequencies in the spectra from location 1 were selected for comparison with natural frequencies of the block. The peaks at 17.46, 21.11, and 40.37 kHz were selected because of their high amplitudes and narrow bandwidths relative to other frequencies. Peaks at 50.95 and 75.64 kHz were chosen arbitrarily to extend the frequency range of comparison. The predominant frequency at 16.42 kHz from location 2 was also selected because of its high amplitude.

Nodal patterns [39-41] were successfully measured for all six selected frequencies, indicating that the six frequencies were natural frequencies of the block. The six natural frequencies corresponded exactly to the values of the peaks obtained from the spectra.

The natural frequency nodal patterns obtained for the six frequencies, shown with the top and side views of the block, are given in Figs. 6 through 11, in order of increasing frequency. The heavy lines within the block perimeter represent the nodal lines. Note that all six of the nodal patterns are symmetrical at least about one axis. Also note that the number of nodal lines increases with increasing frequency, resulting in a closer nodal line spacing.

Nodal lines coincided with the transducer locations for three of the six natural frequencies shown in Figs. 6 through 11. They were 17.46, 21.11, and 75.64 kHz. A nodal line passes through transducer location 2 for both the 17.46 and 21.11 kHz resonant modes. A nodal line passes through transducer location 1 for the 75.64 kHz resonant mode. The sharp reduction in amplitude of the peaks at 17.46 and 21.11 kHz in all spectra from location 2 compared to those from location 1 (Fig. 5) was a result of the transducer being located on a nodal line at location 2. The amplitude of the 17.46 and the 21.11 kHz frequency components in the spectra from location 2 would be zero if the transducer diameter equalled the width of the nodal lines, namely zero diameter. Since the transducer diameter (1.5 cm) was of a greater dimension than the nodal lines, some averaged signal was able to be detected at those frequencies. At higher frequencies such as 75.64 kHz, the spacing of the nodal lines was comparable to the diameter of the transducer. As a consequence, the transducer was responding to both the nodal and antinodal regions on the surface of the test specimen.

Further, it was demonstrated experimentally that the transducer resonant response was not responsible for the spectral content of the output signals or the presence of the nodal patterns [23]. The receiving transducer and the source transducer (used for the nodal pattern measurement) were coupled face-to-face and the voltage amplitude output of the receiving transducer to a 15 V sinusoidal input was recorded. The frequency of the sinusoidal input ranged from 10 to 90 kHz and was incremented in 5 kHz steps. The output voltage of the receiving transducer was a smooth function of frequency. The response curve neither exhibited sharp resonances at any of the six frequencies used for nodal analysis nor did it show a zero (voltage) output that could have been interpreted as a node at any frequency.

The ability to identify natural frequencies of the block, by the measurement of nodal patterns at frequencies corresponding exactly to peaks in the output spectra, clearly supports the statement made earlier that the spectral content of the received

signal is dominated by the natural frequency response of the test specimen. It has been demonstrated that a further influence on the spectral content of the received signal occurs by virtue of the location of the transducer; in particular, the transducer's proximity to a nodal line.

IMPLICATIONS

The spectral content of the received signal has been shown to be dominated by the natural frequency response of the test specimen. It has also been demonstrated that a further influence on the spectral content of the received signal is due to the location of the transducer relative to the natural frequency nodal lines.

Table 1 is a general summary of factors affecting AU parameters and measurements due to the presence of specimen resonances. For example, the measurement of crack growth parameters presents a unique problem in light of the specimen resonant effects presented here. As the crack grows, the geometry of the specimen changes thus shifting the resonant frequencies. Identification of resonant frequencies at the beginning of a crack growth experiment may be of little value by the end of the experiment. An additional consequence of the changing specimen resonances during a crack growth experiment is that the nodal patterns associated with the resonances also change, providing an additional complication. The transducer location might be alternately at a node and an antinode as the crack grows and the geometry changes. Thus, the output signal would reflect the changing nodal patterns in both the time and frequency domains. The presumably abrupt changes in the output signal experienced as such a test progressed could be incorrectly associated with crack growth phenomena.

Table 2 is a summary of AU parameters and measurements affected by the presence of specimen resonances and further influenced by transducer location. Spectral characteristics have been associated with source identification and source alteration [1,21,22]. If the AU source excites resonant frequencies of the test specimen, the spectral characteristics of the output signal may yield significant information about the test specimen resonances but comparatively little information about the source.

AE and UT parameters are affected by specimen resonances and transducer location. A vanishing signal may be obtained from a transducer located on a nodal region of the structure. This results in, for example, small AE ringdown counts, small stress wave factor, and large attenuation. On the other hand, a large signal is obtained from a transducer located on an antinodal region of the same structure. This results in, for example, large AE ringdown counts, large stress wave factor, and small attenuation.

AE source location based on the comparison of AE event arrival times at two or more transducers may also yield misleading results. If the transducers operate at a frequency near a specimen resonance and are located on antinodal regions, AE events may tend to appear to be large in amplitude and long in duration. As the event

duration becomes long, superposition of separate events becomes more likely. The individual identity of events which have been superposed is lost and therefore not available for AE source location.

Further complications can arise due to AE equipment limitations. The event duration may exceed the maximum event duration acceptable by the AE equipment. This will result in the premature truncation of an event by the equipment and possibly the subsequent re-activation of the event duration clock by the same event resulting in an erroneous apparent simultaneous arrival of events. Clearly, these discussions can be extended to include several additional scenarios when some or all of the transducers are located in nodal regions of the structure.

SUGGESTIONS FOR ACOUSTIC-ULTRASONIC TESTING AND REPORTING

Some suggestions for procedures to be followed for AU testing can be made based on the results and implications presented here. A proposed AU test procedure is given in Table 3.

The resonant frequencies and the corresponding nodal patterns of the test specimen should be well characterized within the frequency range to be studied. It is advisable to use the actual test specimen and test configuration (including supports) for the determination of nodal patterns and resonant frequencies. The effects of the changing specimen geometry should also be investigated. After the resonances and mode shapes have been determined, a decision should be made as to whether the resonant frequencies and the associated mode shapes should be avoided or sought during testing. (Resonant frequencies could be desirable for the enhanced signal amplitude that results.) Further, equipment selections should be based on the frequencies to be investigated.

The procedures just suggested for AU testing lead to additional suggestions for test reporting. Table 4 lists the proposed checklist for AU test reporting. The AE checklist presented in [3] has been modified to include information on specimen resonances and other details such as resolution in the frequency domain. The items on the checklist represent a minimum for comparison purposes and consistent reporting.

CONCLUSIONS

The effects of test specimen resonant frequencies on acoustic-ultrasonic (AU) testing have been investigated. The following conclusions can be drawn based on the results, discussion, and implications of this work.

(1) The resonant frequencies of the test specimen dominate the spectral content of the output signal when the input source has energy at the resonant frequencies.

(2) The location of the transducer, relative to the natural frequency nodal lines, further influences the spectral content of the output signal.

(3) Due to the similarity of the sphere impact and pencil lead fracture output signals in both the time and frequency domains, the meanings of statements regarding repeatibility or reproducibility of any AU source must be scrutinized.

(4) Given test specimens of different geometries but identical composition and AU source(s), the spectral content of the output signals will be different.

(5) Given the same AU source(s), specimen material and specimen geometry, different output signals will result from different transducer locations.

(6) Source characterization through frequency signature analysis should be conducted very carefully with full knowledge of specimen and transducer frequency characteristics. Without this knowledge, signature analysis may yield only the resonance signature of the test specimen for the particular transducer location used.

(7) AU parameters and measurements, including ringdown counting, event duration, rise time, peak amplitude, slope, event count, energy, attenuation, stress wave factor and source location, can give misleading results if there is accompanying resonance in the test specimen.

(8) Careful and consistent placement of the transducer on the test specimen is a requirement for the meaningful comparison of results between similar tests.

(9) The AU characterization of crack growth is complicated by changing specimen resonances and nodal patterns as the crack grows.

REFERENCES

[1] R.G. Liptai, D.O. Harris, and C.A. Tatro, ed., Acoustic Emission, ASTM STP 505, American Society for Testing and Materials, Philadelphia, PA, 1972.

[2] J.C. Spanner, Acoustic Emission Techniques and Applications, Intex Publishing Co., Evanston, IL, 1974.

[3] J.H. Williams, Jr., and S.S. Lee, "Acoustic Emission Monitoring of Fiber Composite Materials and Structures", Journal of Composite Materials, Vol. 12, Oct. 1978, pp. 348-370.

[4] S. Kahn and D. Miller, "Acoustic Emission Detection I - Theory, Review of Research and Development, Summary of Western Electric Applications", The Western Electric Engineer, Vol. 23, No. 4, Oct. 1979, pp. 2-14.

[5] T.F. Drouillard, Acoustic Emission - A Bibliography with Abstracts, IFI/Plenum Data Co., NY, 1979.

[6] R.V. Williams, Acoustic Emission, Adam Hilger Ltd., Bristol, England, 1980.

[7] A.E. Lord, Jr., "Acoustic Emission - An Update", Physical Acoustics, Vol. 15, ed. by W.P. Mason and R.N. Thurston, Academic Press, NY, 1981, pp. 295-360.

[8] J.H. Williams, Jr., S.S. Lee, and T.K. Wang, "Quantitative Nondestructive Evaluation of Automotive Glass Fiber Composites", Journal of Composite Materials, Vol. 16, Jan. 1982, pp. 20-39.

[9] J.H. Williams, Jr., D.M. DeLonga, and S.S. Lee, "Correlations of Acoustic Emission with Fracture Mechanics Parameters in Structural Bridge Steels During Fatigue", Materials Evaluation, Vol. 40, No. 11, Oct. 1982, pp. 1184-1189.

[10] J. Krautkramer and H. Krautkramer, Ultrasonic Testing of Materials, 2nd ed., Springer-Verlag, NY, 1977.

[11] R. Truell and A. Hikata, "Fatigue and Ultrasonic Attenuation", Symposium on Nondestructive Testing, ASTM STP 213, American Society for Testing and Materials, Philadelphia, PA, 1957, pp. 63-69.

[12] D.T. Hayford, E.G. Henneke, II, and W.W. Stinchcomb, "The Correlation of Ultrasonic Attenuation and Shear Strength in Graphite Polyimide Composites", Journal of Composite Materials, Vol. 11, Oct. 1977, pp. 429-444.

[13] J.H. Williams, Jr., H. Nayeb-Hashemi, and S.S. Lee, "Ultrasonic Attenuation and Velocity in AS/3501-6 Graphite Fiber Composite", Journal of Nondestructive Evaluation, Vol. 1, No. 2, 1980, pp. 137-148.

[14] J.H. Williams, Jr., and B. Doll, "Ultrasonic Attenuation as an Indicator of Fatigue Life of Graphite Fiber Epoxy Composite", Materials Evaluation, Vol. 38, No. 5, May 1980, pp. 33-37.

[15] J.H. Williams, Jr., and N.R. Lampert, "Ultrasonic Evaluation of Impact-Damaged Graphite Fiber Composite", Materials Evaluation, Vol. 38, No. 12, Dec. 1980, pp. 68-72.

[16] J.H. Williams, Jr., H. Yuce, and S.S. Lee, "Ultrasonic and Mechanical Characterizations of Fatigue States of Graphite Epoxy Composite Laminates", Materials Evaluation, Vol. 40, No. 5, April 1982, pp. 560-565.

[17] A. Vary and R.F. Lark, "Correlation of Fiber Composite Tensile Strength with the Ultrasonic Stress Wave Factor", Journal of Testing and Evaluation, Vol. 7, No. 4, July 1979, pp. 185-191.

[18] A. Vary and K.J. Bowles, "An Ultrasonic-Acoustic Technique for Nondestructive Evaluation of Fiber Composite Quality", Polymer Engineering and Science, Vol. 19, No. 5, April 1979, pp. 373-376.

[19] R.L. Mehan and J.V. Mullin, "Analysis of Composite Failure Mechanisms Using Emissions", Journal of Composite Materials, Vol. 5, April 1971, pp. 266-269.

[20] J.H. Speake and G.J. Curtis, "Characterization of the Fracture Processes in CFRP using Spectral Analysis of the Acoustic Emissions Arising from the Application of Stress", International Conference on Carbon Fibers, Their Place in Modern Technology, London, Feb. 1974, The Plastic Institute, London, Paper No. 29.

[21] W.J. Pardee and L.J. Graham, "Frequency Analysis of Two Types of Simulated Acoustic Emissions", Journal of the Acoustical Society of America, Vol. 63, No. 3, March 1978, pp. 793-799.

[22] N.N. Hsu and S.C. Hardy, "Experiments in Acoustic Emission Waveform Analysis for Characterization of AE Source, Sensors, and Structures", Elastic Waves and Nondestructive Testing of Materials, AMD-Vol. 29, ed. by Y.H. Pao, The American Society of Mechanical Engineers, NY, 1978, pp. 85-106.

[23] E.B. Kahn, "The Effects of Specimen Resonances on Acoustic-Ultrasonic Testing", S.M. Thesis, Department of Mechanical Engineering, Massachusetts Institute of Technology, Cambridge, MA, November 1982.

[24] D.M. Egle and C.A. Tatro, "Analysis of Acoustic-Emission Strain Waves", Journal of the Acoustical Society of America, Vol. 41, No. 2, Feb. 1967, pp. 321-327.

[25] R.W.B. Stephens and A.A. Pollock, "Waveforms and Frequency Spectra of Acoustic Emissions", Journal of the Acoustical Society of America, Vol. 50, No. 3, Sept. 1971, pp. 904-910.

[26] L.J. Graham and G.A. Alers, "Spectrum Analysis of Acoustic Emission in A533-B Steel", Materials Evaluation, Vol. 32, No. 2, Feb. 1974, pp. 31-37.

[27] G. Curtis, "Acoustic Emission-4, Spectral Analysis of Acoustic Emission", Non-Destructive Testing, Vol. 7, No. 2, April 1974, pp. 82-91.

[28] D.M. Egle and A.E. Brown, "Considerations for the Detection of Acoustic Emission Waves in Thin Plates", Journal of the Acoustical Society of America, Vol. 57, No. 3, March 1975, pp. 591-597.

[29] P. Fleischman, D. Rouby, F. Lakestani, and J.C. Baboux, "A Spectrum Analysis of Acoustic Emission", Non-Destructive Testing, Vol. 8, No. 5, Oct. 1975, pp. 241-244.

[30] K. Ono and J. Ucisik, "Acoustic Emission Behavior of Aluminum Alloys", Materials Evaluation, Vol. 34, No. 2, Feb. 1976, pp. 32-44.

[31] S.D. Stearns, Digital Signal Analysis, Hayden Book Co., Rochelle Park, NJ, 1975.

[32] C.M. Rabiner and B. Gold, Theory and Application of Digital Signal Processing, Prentice-Hall Inc., Englewood Cliffs, NJ, 1974.

[33] A.V. Oppenheim and R.W. Schafer, Digital Signal Processing, Prentice-Hall Inc., Englewood Cliffs, NJ, 1975.

[34] W. Goldsmith, Impact: The Theory and Physical Behavior of Colliding Solids, Edward Arnold, Ltd., London, 1960.

[35] C.V. Raman, "On Some Applications of Hertz's Theory of Impact", Physical Review, Series 2, Vol. 15, No. 4, April 1920, pp. 277-284.

[36] N.N. Hsu, Acoustic Emission Simulator, U.S. Patent 4018084 assigned to Lockheed Aircraft Corporation, Burbank, CA, May 1976.

[37] N.N. Hsu, J.A. Simmions, and S.C. Hardy, "An Approach to Acoustic Emission Signal Analysis", Materials Evaluation, Vol. 35, No. 11, Oct. 1977, pp. 100-106.

[38] L.R. Rabiner, R.W. Schafer, and D. Dlugos, "Correlation Method for Power Spectrum Estimation", Programs for Digital Signal Processing, ed. by the Digital Signal Processing Committee, IEEE Acoustics, Speech, and Signal Processing Society, IEEE Press, John Wiley and Sons, Inc., NY, 1979, pp. 2.2-13-2.2-14.

[39] P.M. Morse, Vibration and Sound, 2nd ed., McGraw-Hill Book Co., NY, 1948.

[40] M.D. Waller, Chladni Figures, A Study in Symmetry, G. Bell and Sons, Ltd., London, 1961.

[41] A.W. Leissa, Vibration of Plates, NASA SP-160, National Aeronautics and Space Administration, Washington, D.C., 1969.

TABLE 1 Factors Affecting AU Parameters and Measurements Due to the Presence of Specimen Resonances

Material
Specimen geometry (as modified by deformation during crack growth, corrosion or creep tests)
Transducer location
Transducer characteristics

TABLE 2 AU Parameters and Measurements Affected by the Presence of Specimen Resonances and Further Influenced by Transducer Location

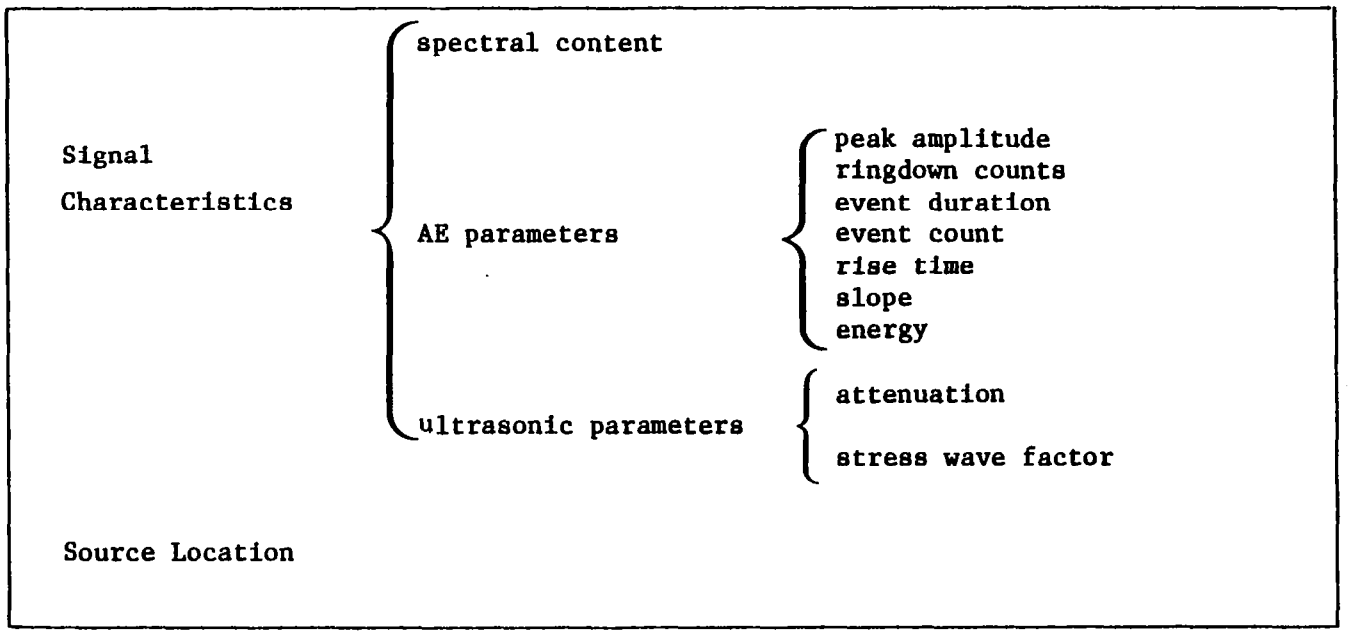

TABLE 3 Proposed AU Test Procedure

1. Determine specimen resonant frequencies within the frequency range to be studied.
2. Determine corresponding nodal patterns.
3. Investigate effects of changing specimen geometry on resonant frequencies and mode shapes if appropriate (cracks, corrosion, creep).
4. Determine whether specimen resonances are to be avoided or sought.
5. Select transducer based on frequency characteristics.
6. Select transducer location based on mode shapes and step 4.
7. Select appropriate measurement equipment.

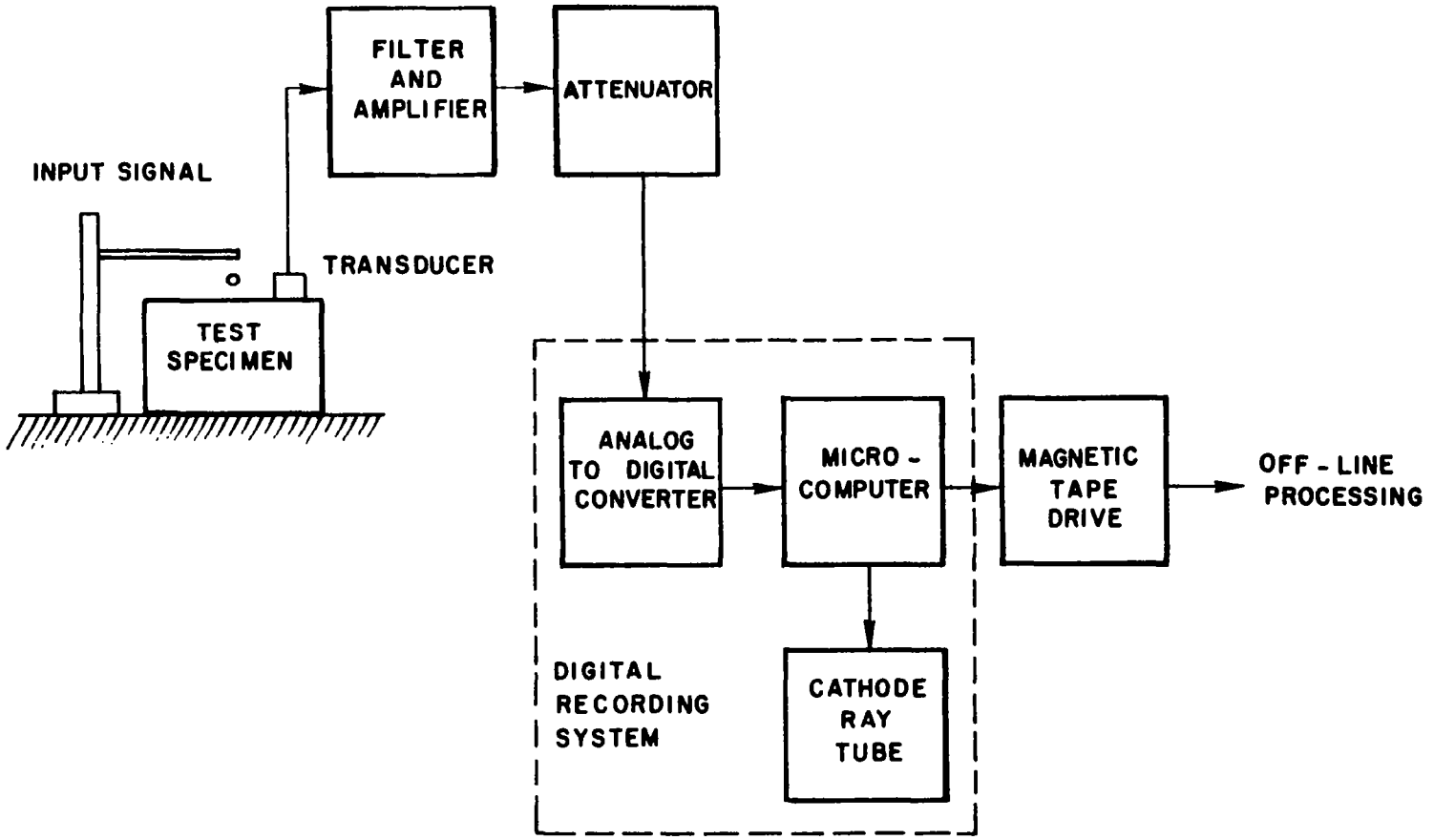

Fig. 2 Schematic of the experimental system for measurement of the specimen response to the fracture of pencil lead and the impact of spheres.

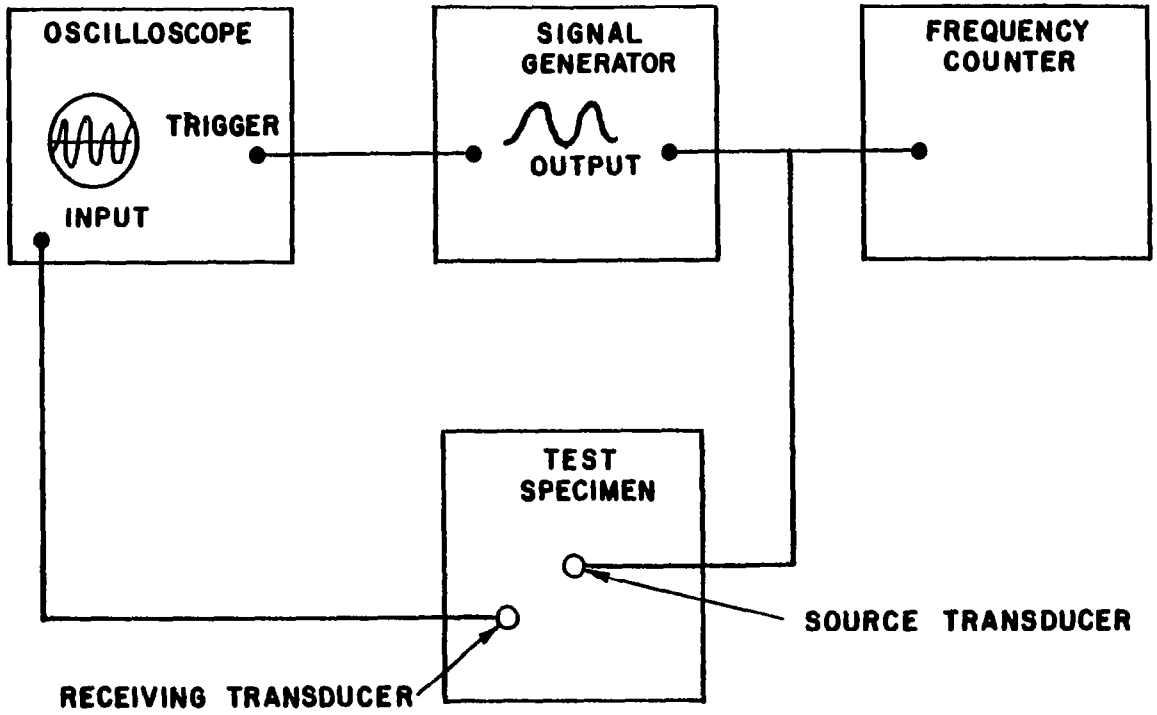

Fig. 3 Schematic of the experimental system for the measurement of nodal patterns.

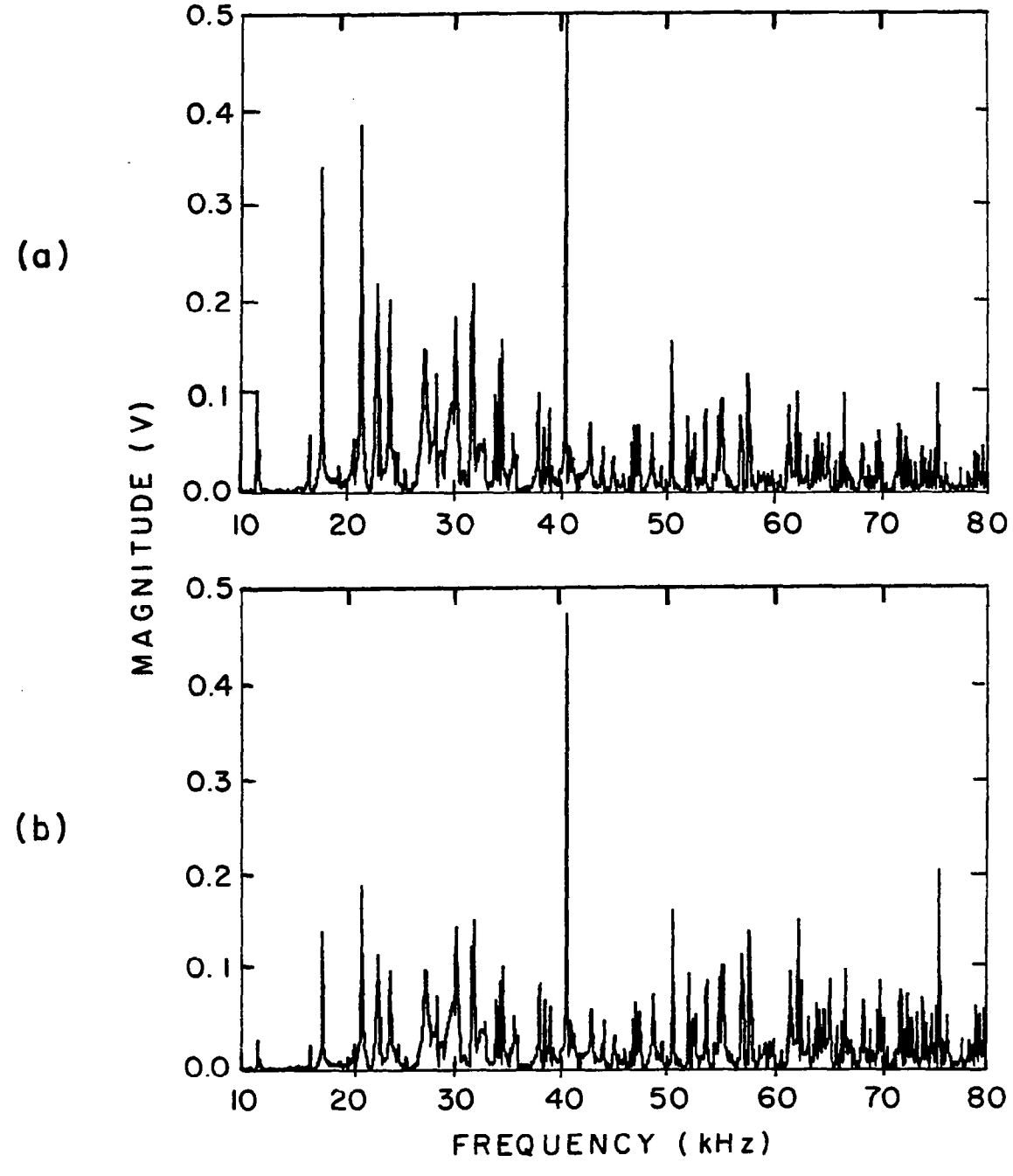

Fig. 4 Spectra obtained at output transducer location 1, from 10 to 80 kHz, for (a) pencil lead fracture and (b) 0.159 cm (1/16 in) diameter sphere impact signals.

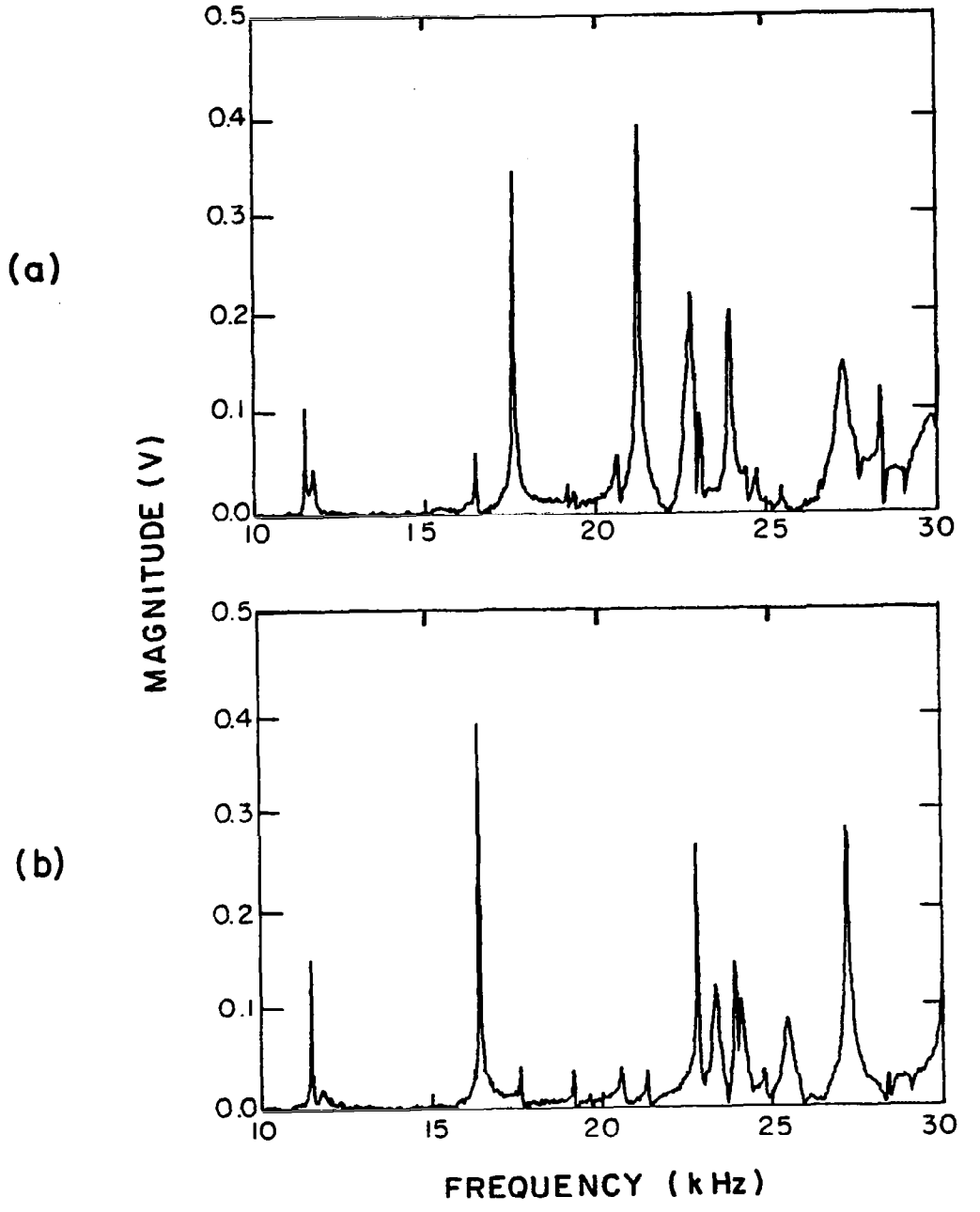

Fig. 5 Spectra obtained for pencil lead fracture signals, from 10 to 30 kHz, at output transducer (a) location 1 and (b) location 2.

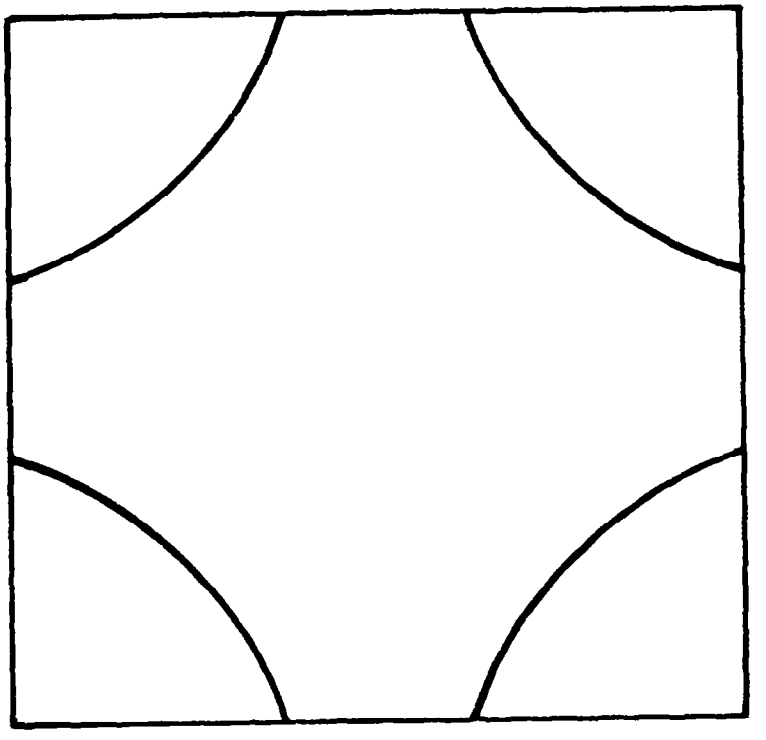

Fig. 6 Nodal pattern measured at the resonant frequency of 16.42 kHz.

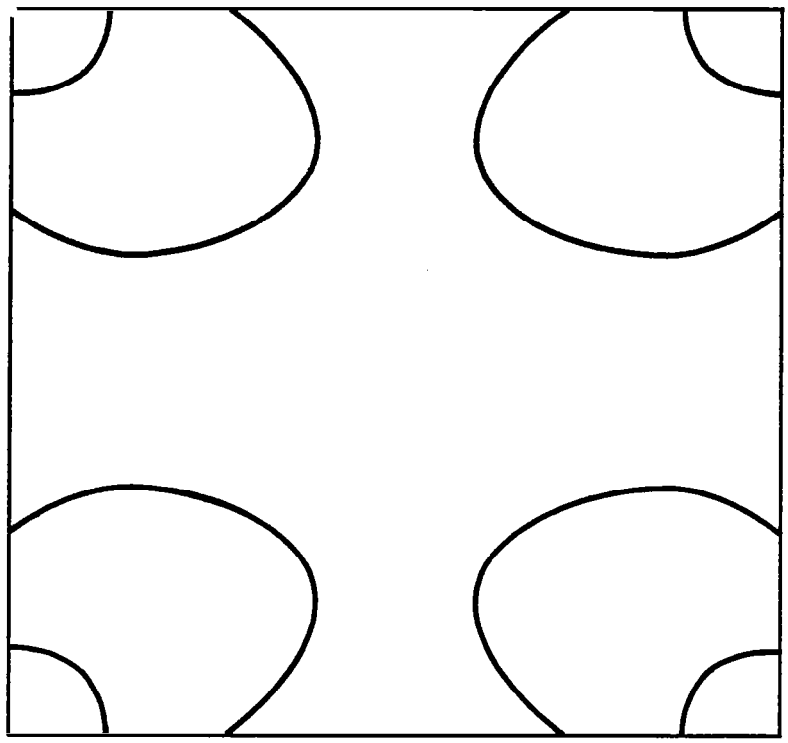

TOP VIEW

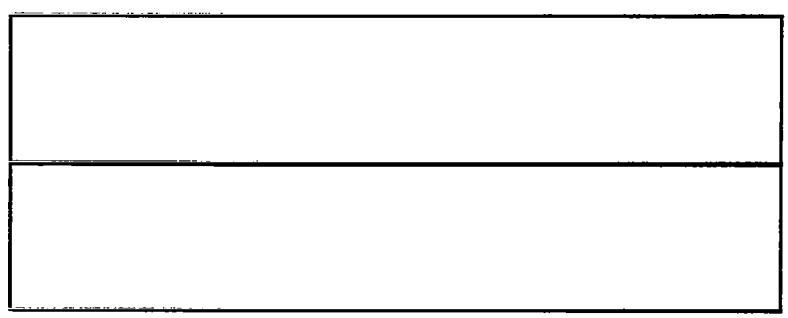

SIDE VIEW

Fig. 7 Nodal pattern measured at the resonant frequency of 17.46 kHz.

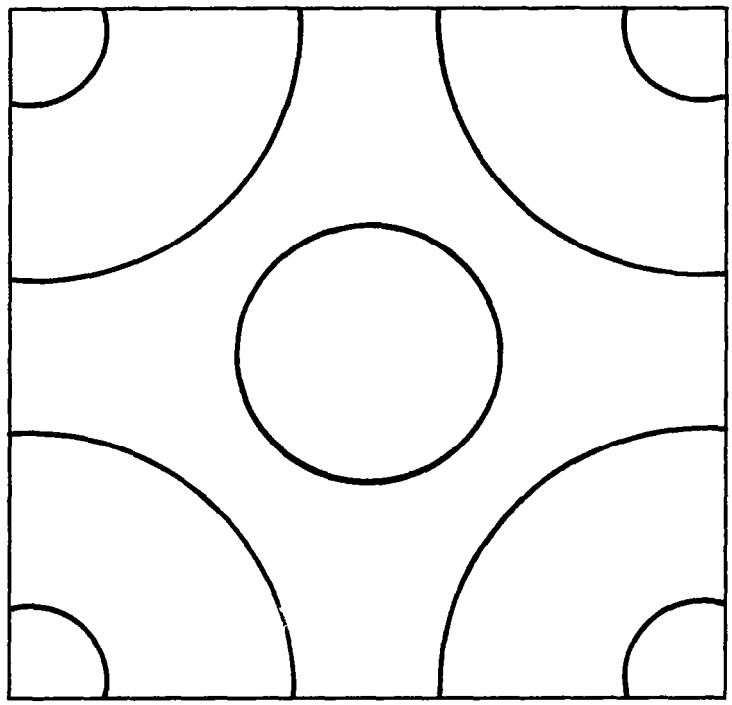

TOP VIEW

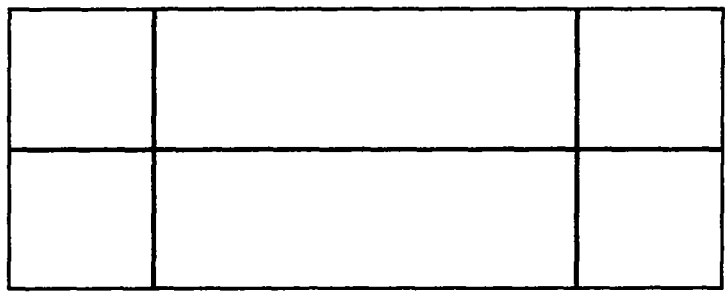

SIDE VIEW

Fig. 8 Nodal pattern measured at the resonant frequency of 21.11 kHz.

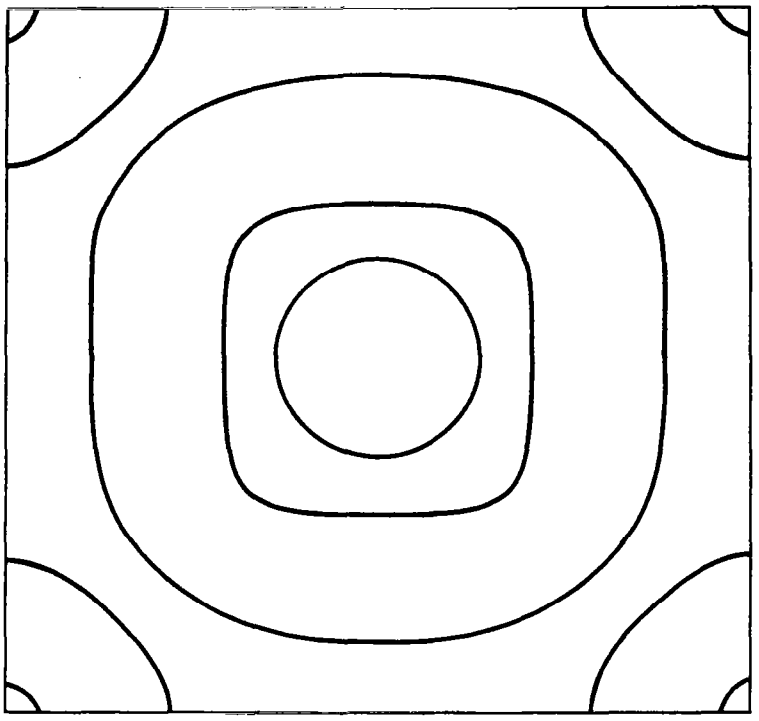

TOP VIEW

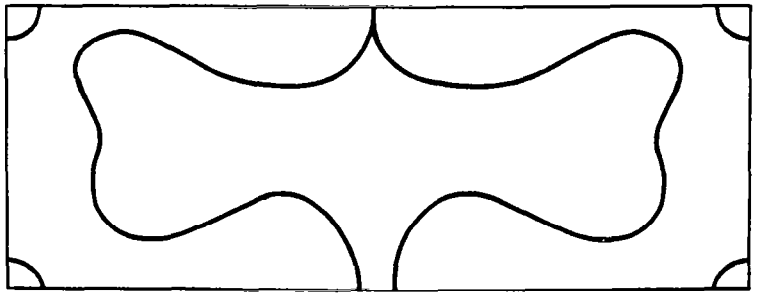

SIDE VIEW

Fig. 9 Nodal pattern measured at the resonant frequency of 40.37 kHz.

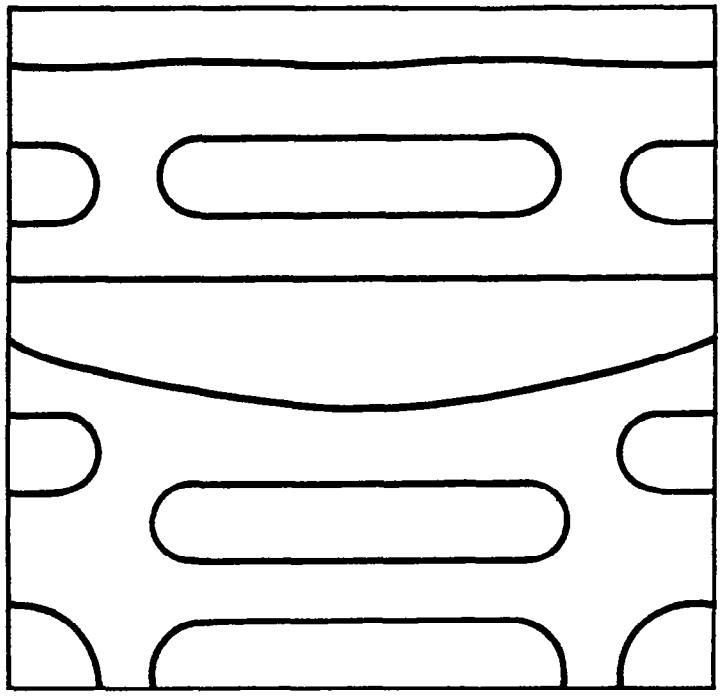

Fig. 10 Nodal pattern measured at the resonant frequency of 50.95 kHz.

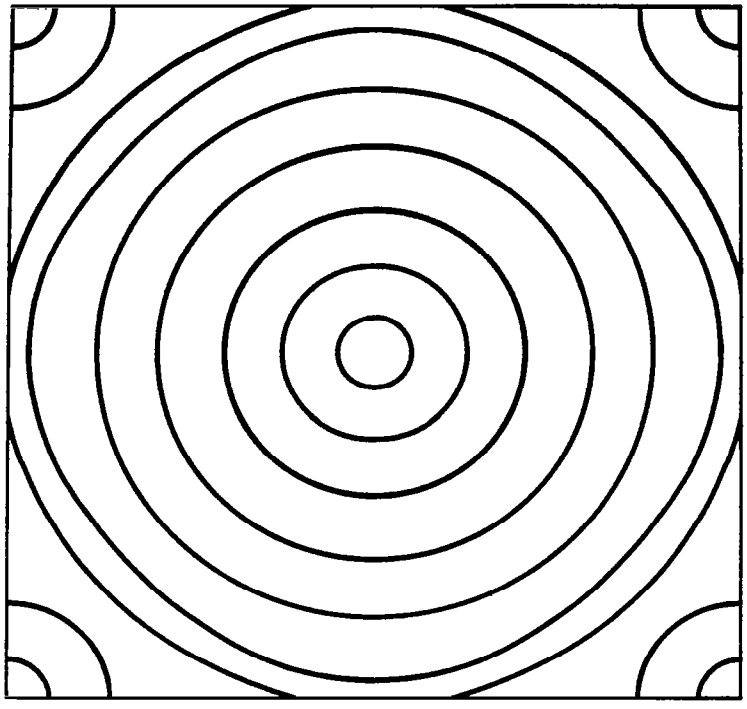

TOP VIEW

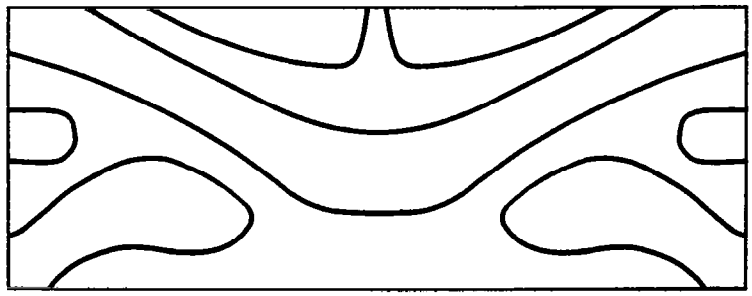

SIDE VIEW

Fig. 11 Nodal pattern measured at the resonant frequency of 75.64 kHz.

1. Report No.	2. Government Accession No.	3. Recipient's Catalog No.
NASA CR-3679		

4. Title and Subtitle	5. Report Date
EFFECTS OF SPECIMEN RESONANCES ON ACOUSTIC-ULTRASONIC TESTING	March 1983
	6. Performing Organization Code

7. Author(s)	8. Performing Organization Report No.
James H. Williams, Jr., Elsbeth B. Kahn, and Samson S. Lee	None
	10. Work Unit No.

9. Performing Organization Name and Address	11. Contract or Grant No.
Massachusetts Institute of Technology Department of Mechanical Engineering Cambridge, Massachusetts 02139	NSG-3210
	13. Type of Report and Period Covered
12. Sponsoring Agency Name and Address	Contractor Report
National Aeronautics and Space Administration Washington, D. C. 20546	14. Sponsoring Agency Code 505-33-22 (E-1552)

15. Supplementary Notes

Final report. Project Manager, Alex Vary, Materials Division, NASA Lewis Research Center, Cleveland, Ohio 44135.

16. Abstract

The effects of specimen resonances on acoustic-ultrasonic (AU) nondestructive testing are investigated. The frequency responses in the range of 10 to 280 kHz of a 25.4- by 25.4- by 10.2-cm (10- by 10- by 4-in.) solid 6061-T6 aluminum block to the fracture of a 0.5-mm (0.02-in.) diameter HB type pencil lead and to the impact of 0.159-cm (1/16-in.) and 0.318-cm (1/8-in.) diameter stainless steel spheres are obtained at two different transducer locations. Selected resonant frequencies and the corresponding normal mode nodal patterns of the aluminum block are measured up to 75.64 kHz. Prominent peaks in the pencil lead fracture and sphere impact spectra from the two transducer locations corresponded exactly to resonant frequencies of the block. Thus, it is established that the resonant frequencies of the block dominated the spectral content of the output signal. The spectral content of the output signals is further influenced by the transducer location relative to the resonant frequency nodal lines, Implications of the results are discussed in relation to AU parameters and measurements. An AU test procedure as well as a checklist for AU test reporting are proposed.

17. Key Words (Suggested by Author(s))	18. Distribution Statement
Nondestructive testing; Ultrasonics; Acoustics; Spectrum analysis; Signature analysis; Resonance; Acoustic emission; Ultrasonic transducers	Unclassified - unlimited STAR Category 38

19. Security Classif. (of this report)	20. Security Classif. (of this page)	21. No. of Pages	22. Price*
Unclassified	Unclassified	35	A03

* For sale by the National Technical Information Service, Springfield, Virginia 22161

NASA-Langley, 1983